Spectral kinetic energy transfer in turbulent premixed reacting flows

C. A. Z. Towery,[1] A. Y. Poludnenko,[2] J. Urzay,[3] J. O'Brien,[3] M. Ihme,[3] and P. E. Hamlington[1,*]
[1]*Department of Mechanical Engineering, University of Colorado, Boulder, Colorado 80309, USA*
[2]*Laboratories for Computational Physics and Fluid Dynamics, Naval Research Laboratory, Washington, D.C. 20375, USA*
[3]*Center for Turbulence Research, Stanford University, Stanford, California 94305, USA*
(Received 30 December 2015; revised manuscript received 1 April 2016; published 23 May 2016)

Spectral kinetic energy transfer by advective processes in turbulent premixed reacting flows is examined using data from a direct numerical simulation of a statistically planar turbulent premixed flame. Two-dimensional turbulence kinetic-energy spectra conditioned on the planar-averaged reactant mass fraction are computed through the flame brush and variations in the spectra are connected to terms in the spectral kinetic energy transport equation. Conditional kinetic energy spectra show that turbulent small-scale motions are suppressed in the burnt combustion products, while the energy content of the mean flow increases. An analysis of spectral kinetic energy transfer further indicates that, contrary to the net down-scale transfer of energy found in the unburnt reactants, advective processes transfer energy from small to large scales in the flame brush close to the products. Triadic interactions calculated through the flame brush show that this net up-scale transfer of energy occurs primarily at spatial scales near the laminar flame thermal width. The present results thus indicate that advective processes in premixed reacting flows contribute to energy backscatter near the scale of the flame.

DOI: 10.1103/PhysRevE.93.053115

I. INTRODUCTION

Improved understanding of turbulence-flame interactions is required for the development of more accurate models of subgrid-scale (SGS) dynamics in large eddy simulations (LES) of premixed reacting flows. These interactions are nonlinear, occur over a wide range of scales, and challenge many of the principal assumptions of classical turbulence and combustion theories [1,2]. In particular, kinetic energy transfer in premixed reacting flows may dominantly occur from small to large scales as a result of chemical heat release by the flame, contrary to the net transfer of energy from large to small scales found in many nonreacting flows.

There are a number of ways in which a premixed flame may affect the energetics of a turbulent flow. For example, the increase in temperature due to heat release raises the gas viscosity, thereby lowering the local Reynolds number and causing kinetic energy dissipation to occur at larger spatial scales. Similarly, the gas density decreases as the temperature rises, resulting in fluid expansion and acceleration of the flow through the flame. This, in turn, results in changes to pressure-gradient work and dilatational effects in the flow, both of which provide a direct path from small-scale heat release by the flame to enhancement of large-scale turbulence kinetic energy [3].

In the present study, we specifically examine the effects of premixed flames on interscale kinetic energy transfer by nonlinear advective processes. From a spectral standpoint, advection is responsible for the transfer of energy between groups of three different wave vectors, and the resulting multiscale interactions are termed triadic interactions [4–9]. These interactions result in both down-scale (i.e., large to small scale) and up-scale (i.e., small to large scale) energy transfer, which can be local, nonlocal, or distant in scale space [6,7,9]. In many nonreacting and incompressible turbulent flows, local down-scale energy transfer dominates other interactions throughout the inertial range. This imbalance results in the net forward (i.e., down-scale) kinetic energy cascade that is the basis for most classical theories of turbulence, including the theory proposed by Kolmogorov [10].

Our focus here is on understanding how the balance between down-scale and up-scale kinetic energy transfer changes in turbulent premixed reacting flows, and whether there is a net up-scale transfer of energy associated with advective processes. Such a net up-scale energy transfer could be considered a particular type of energy "backscatter." Furthermore, if such net advective backscatter does exist, we seek to characterize the range of scales over which it occurs. In particular, net up-scale energy transfer over a wide range of scales extending from the scale of the flame width to the turbulent integral scale would be indicative of an extended inverse energy cascade, contrary to the net forward energy cascade found in most three-dimensional (3D) nonreacting flows.

Some of the earliest attempts to understand the effects of flames on turbulence spectra were made experimentally by Furukawa *et al.* [11,12], who found that small-scale motions in the product gases outside of a thin premixed flame are suppressed relative to motions in the reactant gases. More recently, Knaus and Pantano [1] calculated velocity and scalar spectra using direct numerical simulations (DNS) of nonpremixed flames, showing that density-weighted spectra collapse to classical predictions for nonreacting turbulence made by Kolmogorov [10]. Kolla *et al.* [2] computationally examined density-weighted kinetic energy and scalar spectra using DNS of a premixed shear-driven turbulent flame and showed that these spectra only collapse to classical Kolmogorov predictions at intermediate scales far from the scale of the flame width. Relatively few prior attempts have been made to specifically study advective transfer and backscatter in reacting flows. O'Brien *et al.* [3,13] performed computational, physical-space analyses of energy transfer between subfilter and resolved scales in the compressible, Favre-filtered Navier-Stokes equations. By applying differential filters of many

*peh@colorado.edu

widths to DNS data of both diffusion [13] and premixed [3] flames, it was found that subfilter-scale backscatter occurs primarily in regions undergoing dilatation due to heat release.

Despite the insights provided by these prior studies, there is still incomplete understanding of how heat release affects advective kinetic energy transfer within a spectral framework. In the present study, spectral kinetic energy (SKE) transfer by advective processes is examined using two-dimensional (2D) Fourier spectra conditioned on the planar-averaged reactant mass fraction to indicate location in the flame brush. Here the flame brush is defined as the spatial region that fully encompasses the turbulent premixed flame. The analysis is based on data from a new high-resolution DNS of a statistically planar premixed flame in an unconfined domain. The canonical nature of this configuration, which has also been examined previously in other studies (see, for instance, Refs. [14] and [15]), allows turbulence-flame interactions to be examined in the absence of additional complicating physical effects, such as mean shear. Moreover, in this configuration, the two spatial dimensions normal to the direction of mean flame propagation are homogeneous, isotropic, and have periodic boundary conditions. This permits a conditional Fourier analysis in 2D planes through the flame brush, which is inhomogeneous in the third dimension. Even though both the turbulence and the flame are inherently 3D, no loss of information or degrees of freedom in the dynamics is incurred by applying a 2D Fourier transform to 3D transport equations. As a result, the present 2D Fourier analysis provides physical insights into spectral variations through the flame brush and also permits the calculation of triadic interactions between turbulent scales of motion.

It should be noted that this study is not the first to use a 2D analysis for the study of triadic interactions in a 3D turbulent flow that is homogeneous in two dimensions and inhomogeneous in the third dimension. Most notably, Domaradzki *et al.* [8] performed an analysis of spectral energy transfer and triadic interactions in a turbulent channel flow, using a similar 2D approach to that employed here. The use of 2D conditional statistics for the study of turbulent flow structure and scales of motion in a reacting flow is similarly not new. In particular, Kolla *et al.* [2] performed a conditional analysis of velocity and reactive scalar spectra in the flame brush of a premixed shear-driven turbulent reacting flow. In their study, one-dimensional (1D) spectra were averaged in 2D planes in which the flow was homogeneous, and conditional statistics were computed based on the average value of the combustion progress variable within each plane.

In the following, details of the numerical simulation are described first, followed by the formulation of the SKE transport equation and a description of how interscale advective kinetic energy transfer can be characterized in premixed reacting flows, particularly through the calculation of triadic interactions. Results from the DNS are then presented and conclusions are provided at the end.

II. DETAILS OF THE NUMERICAL SIMULATION

The present analysis is based on data from a new turbulent premixed reacting flow DNS performed using the code ATHENA-RFX [16–18]. The simulation solves the reactive flow equations given by

$$\frac{\partial \rho}{\partial t} + \frac{\partial}{\partial x_j}(\rho u_j) = 0, \tag{1}$$

$$\frac{\partial(\rho u_i)}{\partial t} + \frac{\partial}{\partial x_j}\Bigg[\rho u_i u_j + p\delta_{ij} - 2\mu\left(S_{ij} - \frac{1}{3}S_{kk}\delta_{ij}\right) - \frac{5}{3}\mu S_{kk}\delta_{ij}\Bigg] = \mathcal{F}_i, \tag{2}$$

$$\frac{\partial(\rho e_0)}{\partial t} + \frac{\partial}{\partial x_j}\Bigg[\rho e_0 u_j + p u_j - k\frac{\partial \vartheta}{\partial x_j} - 2\mu u_i\left(S_{ij} - \frac{1}{3}S_{kk}\delta_{ij}\right) - \frac{5}{3}\mu u_j S_{kk}\Bigg] = -\rho q \dot{w} + u_i \mathcal{F}_i, \tag{3}$$

$$\frac{\partial(\rho Y)}{\partial t} + \frac{\partial}{\partial x_j}\left(\rho Y u_j - \lambda\frac{\partial Y}{\partial x_j}\right) = \rho\dot{w}, \tag{4}$$

where u_i is the velocity vector, ρ is the density, p is the pressure, e_0 is the specific total energy, ϑ is the temperature, Y is the reactant mass fraction (where $Y = 1$ in the reactants and $Y = 0$ in the products), $S_{ij} = \frac{1}{2}(\partial u_i/\partial x_j + \partial u_j/\partial x_i)$ is the strain rate, and thermodynamic variables are related to each other by the ideal gas equation of state. The shear viscosity is denoted μ, the bulk viscosity has been set equal to $\frac{5}{3}\mu$ (giving a second coefficient of viscosity equal to μ), the mass diffusivity is denoted λ, and k is the thermal conductivity. Each of the transport coefficients has a power-law dependence on temperature ϑ given by

$$\mu = \rho_r \nu_r (\vartheta/\vartheta_r)^n, \tag{5}$$

$$k = \rho_r \alpha_r c_p (\vartheta/\vartheta_r)^n, \tag{6}$$

$$\lambda = \rho_r \mathsf{D}_r (\vartheta/\vartheta_r)^n. \tag{7}$$

Here n is a constant, ν_r, α_r, and D_r are the kinematic viscosity, thermal diffusivity, and mass diffusivity at the unburnt reactant conditions ϑ_r and ρ_r, and $c_p = \gamma R/M(\gamma - 1)$ is the specific heat capacity at constant pressure. The Lewis number in the present DNS, $\mathrm{Le} = \alpha_r/\mathsf{D}_r$, is unity. The reaction rate, $\dot{w}$, is modeled using first-order, single-step Arrhenius kinetics as

$$\dot{w} = -\rho Y B \exp\left(-\frac{Q}{RT}\right), \tag{8}$$

where B is the pre-exponential factor and Q is the activation energy. The corresponding chemical energy release is denoted q. The single-step reaction model used here provides realistic predictions of flame structure and heat release [17,19] while maintaining low computational cost, thereby allowing the high spatial resolution achieved in the present DNS. Finally, homogeneous isotropic turbulence (HIT) in the inert reactants is sustained through a large-scale isotropic forcing term $\mathcal{F}_i$, as described in Ref. [17]. A separate simulation of inert HIT in a cubic, periodic domain was performed to serve as a baseline for comparison with premixed reacting flow results. Values of all simulation parameters for both the flame and inert HIT are provided in Table I.

TABLE I. Input model parameters and resulting laminar and turbulent flame properties for the premixed flame DNS.

L	0.259 cm	Domain width, turbulence forcing scale
ϑ_r	293 K	Initial temperature
p_r	1.01×10^6 erg/cm^3	Initial pressure
ρ_r	8.73×10^{-4} g/cm^3	Initial density
γ	1.17	Adiabatic index
M	21 g/mol	Molecular weight
ϑ_p	2135 K	Post-flame temperature
ρ_p	1.2×10^{-4} g/cm^3	Post-flame density
B	6.85×10^{12} cm^3/(g s)	Pre-exponential factor
Q	46.37 $R\vartheta_r$	Activation energy
q	43.28 $R\vartheta_r/M$	Chemical energy release
ν_r	0.189 cm^2/s	Initial kinematic viscosity
α_r	1.77 cm^2/s	Initial thermal diffusivity
D_r	1.77 cm^2/s	Initial mass diffusivity
n	0.7	Temperature exponent
δ_L	0.032 cm	Laminar flame thermal width
S_L	302 cm/s	Laminar flame speed
ℓ	0.060 cm	Integral length scale in reactants
U_ℓ	751 cm/s	Integral velocity scale in reactants
τ_ed	8.27×10^{-5} s	Turbulent eddy-turnover time
Da	0.77	Damköhler number
Ka	20.3	Karlovitz number
$\mathrm{Ma}_{T,r}$	0.03	Initial turbulence Mach number

The physical configuration examined here is that of a turbulent premixed flame in an unconfined domain. The computational domain is discretized using a uniform grid of size $512 \times 512 \times 16\,384$. The simulation is initiated without a flame and turbulence forced at the scale of the domain width, $L = L_{x_1} = L_{x_2}$, develops over five eddy-turnover times. The eddy-turnover time is defined here in terms of the turbulent integral length, ℓ, and velocity, U_ℓ, scales as $\tau_\mathrm{ed} \equiv \ell/U_\ell$. After this spin-up phase, a planar laminar flame is initialized in the domain and a turbulent flame is allowed to develop for an additional five eddy-turnover times. Subsequently, data are collected for the spectral analysis over roughly two and a half eddy-turnover times during which the turbulent flame speed and global kinetic energy remain approximately constant, giving statistically stationary data. Periodic boundary conditions are used in the x_1 and x_2 directions, resulting in flow homogeneity in x_1-x_2 planes and a statistically planar flame. Boundaries in the x_3 direction are periodic prior to ignition and open after ignition. The mean flame normal direction is along the x_3 axis, which is also the direction of the mean flow generated by fluid expansion due to heat release in the flame. The domain is much longer in the x_3 direction, $L_{x_3} = 32L$, in order to allow sufficient space for the flame to be initialized and to propagate for many eddy-turnover times without leaving the domain through either of the x_3 boundaries.

The reactive mixture considered here has laminar flame properties similar to those of an atmospheric, stoichiometric H_2-air flame [17,19]. In particular, the laminar flame speed is $S_\mathrm{L} = 302$ cm/s and the laminar flame thermal width is $\delta_\mathrm{L} \equiv (\vartheta_p - \vartheta_r)/(d\vartheta/dx)_{\mathrm{L,max}} = 0.032$ cm, where $\vartheta_p = 2135$ K is the burnt products temperature, $\vartheta_r = 293$ K is the unburnt reactants temperature, and $(d\vartheta/dx)_{\mathrm{L,max}}$ is the maximum temperature gradient in the laminar flame. Turbulence conditions correspond to the thin reaction zones regime [20] with Damköhler number $\mathrm{Da} = 0.77$ and Karlovitz number $\mathrm{Ka} = 20.3$; the corresponding location of the present DNS on the combustion regime diagram is shown in Fig. 1. Here Da and Ka are defined using the laminar flame thermal width δ_L, the laminar flame speed S_L, and the integral length and velocity scales in the reactants, ℓ and U_ℓ, as

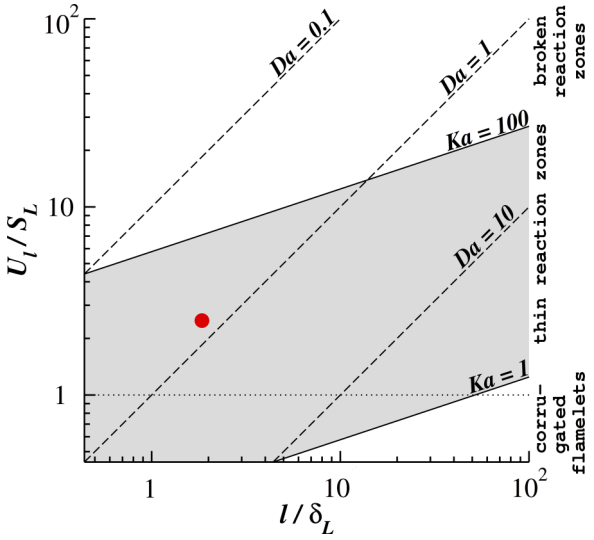

FIG. 1. Combustion regime diagram [20] showing the location of the present DNS within the thin reaction zones regime. The Damköhler (Da) and Karlovitz (Ka) numbers are defined in Eqs. (9) and (10), respectively.

$$\mathrm{Da} \equiv \frac{\tau_\mathrm{ed}}{\tau_\mathrm{C}} = \left(\frac{\ell}{\delta_\mathrm{L}}\right)\left(\frac{U_\ell}{S_\mathrm{L}}\right)^{-1}, \tag{9}$$

$$\mathrm{Ka} \equiv \frac{\tau_\mathrm{C}}{\tau_\mathrm{K}} = \left(\frac{S_\mathrm{L}\delta_\mathrm{L}}{\nu_r}\right)^{1/2}\left(\frac{\ell}{\delta_\mathrm{L}}\right)^{-1/2}\left(\frac{U_\ell}{S_\mathrm{L}}\right)^{3/2}, \tag{10}$$

where $\tau_\mathrm{C} \equiv \delta_\mathrm{L}/S_\mathrm{L}$ is the chemical time scale, and $\tau_\mathrm{ed} \equiv \ell/U_\ell$ and $\tau_\mathrm{K} \equiv (\nu_r/\varepsilon)^{1/2}$ are the eddy turnover and Kolmogorov timescales, respectively, in the unburnt reactants. Using classical scaling arguments, it is assumed in obtaining Eq. (10) that the kinetic energy dissipation rate ε is given as $\varepsilon = U_\ell^3/\ell$ in the unburnt reactants.

The DNS is well resolved, with 64 computational cells spanning one δ_L and two grid cells spanning the Kolmogorov length, $\widetilde{\eta}_\mathrm{K} = (\widetilde{\nu}^3/\widetilde{\varepsilon})^{1/4}$, in the unburnt reactants. There are 25 grid cells per $\widetilde{\eta}_\mathrm{K}$ in the burnt products far from the flame brush. Here $\widetilde{\nu} \equiv \langle \mu \mid \overline{Y}\rangle/\langle \rho \mid \overline{Y}\rangle$ is the average kinematic viscosity and $\widetilde{\varepsilon} \equiv \langle \rho\varepsilon \mid \overline{Y}\rangle/\langle \rho \mid \overline{Y}\rangle$ is the average kinetic energy dissipation rate (see Sec. III for definitions of averaging operators). It should be noted that the spatial resolution of the present DNS is four times greater than recommendations for both fully resolved turbulence [2,21] and fully resolved premixed flames [17], thereby providing confidence in the physical accuracy of the DNS results presented herein.

Figure 2 shows the resulting turbulent flame structure at one instant from the DNS. Comparison of Figs. 2(a) and 2(b) shows that, although the flame is wrinkled and affected by the turbulent flow throughout, the flame is wrinkled at

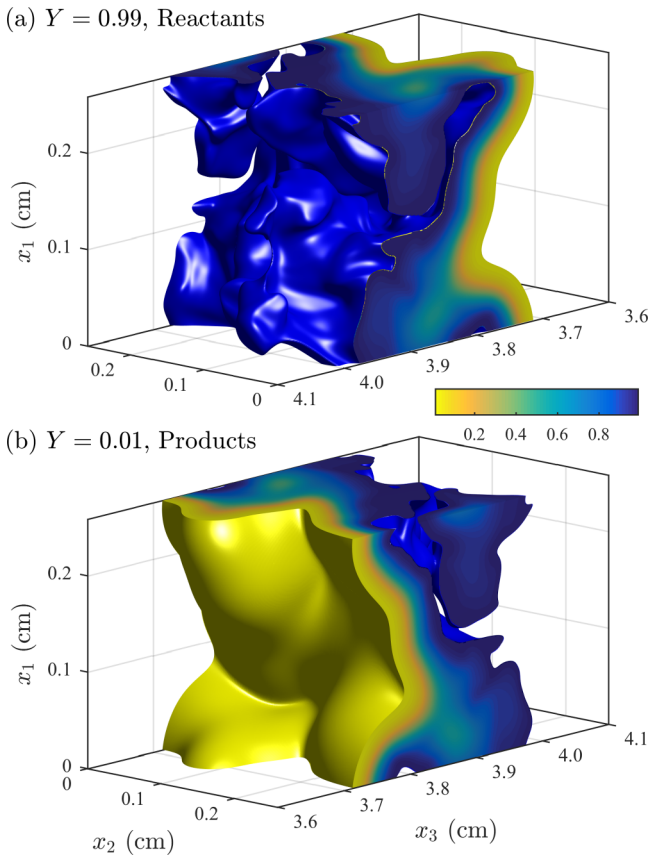

FIG. 2. Structure of the turbulent premixed flame at one instant from the DNS. Panel (a) shows the $Y = 0.99$ isosurface near the reactants and (b) shows the $Y = 0.01$ isosurface near the products. Colors indicate the value of Y within the flame. Note that only the computational domain in the vicinity of the flame is shown.

smaller scales near the reactants than near the products. This is consistent with prior studies of turbulent premixed flames [17,22] using the same computational code. Moreover, while the DNS resolves δ_L with 64 computational cells, the turbulent flame structure shown in Fig. 2 spans nearly 600 computational cells in the x_3 direction, and thus there is considerable spatial resolution within the turbulent flame brush.

Figure 3 shows cross-sectional fields of dilatation S_{kk}, specific kinetic energy $\frac{1}{2}u_i u_i$, and vorticity magnitude $\sqrt{\omega_i \omega_i}$ at one instant from the DNS, where the vorticity is defined using the alternating tensor ϵ_{ijk} as $\omega_i = \epsilon_{ijk}\partial u_k/\partial x_j$. Figure 3(a) shows that dilatation is strongest near the premixed flame, while Fig. 3(b) shows that there is an increase in kinetic energy from the reactants to the products due to the increase in u_3 as a result of fluid expansion. Figure 3(c) shows that there is a large suppression of vorticity magnitude across the flame, most likely due to the combined effects of dilatation and increasing viscosity.

The physical model, numerical algorithms, and simulation setup used here have also been described in prior studies of turbulent flames in Refs. [17,18,22–24]. In particular, Refs. [17,18] and [24] compare the single-step chemistry model to theoretical predictions of the turbulent flame speed and provide a convergence study for the laminar flame thermal width resolution. Additionally, the new simulation discussed

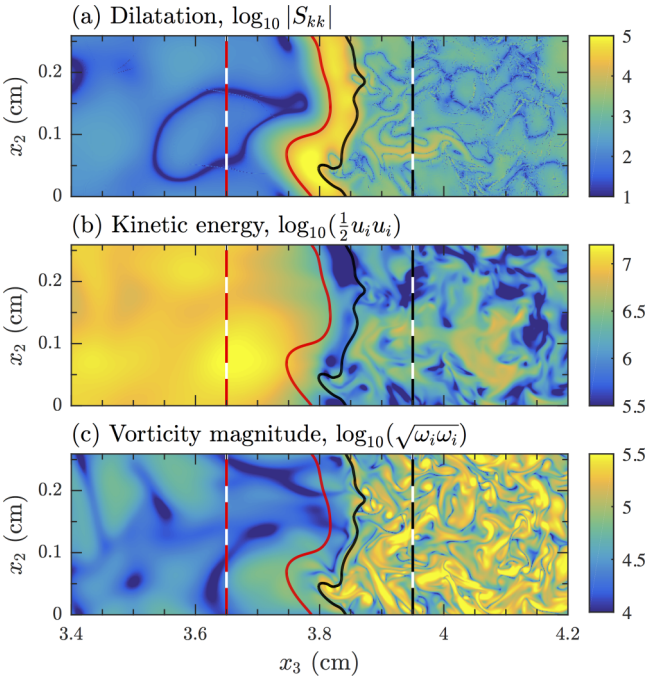

FIG. 3. Instantaneous x_2-x_3 fields from the premixed flame DNS. The panels show (a) dilatation S_{kk}, (b) specific kinetic energy $\frac{1}{2}u_i u_i$, and (c) vorticity magnitude $\sqrt{\omega_i \omega_i}$. Solid red (gray) lines in (a)–(c) are the contour $Y = 0.05$, solid black lines are $Y = 0.95$, and red (gray) and black dashed lines are the boundaries of the flame brush, corresponding to $0.005 \leqslant \overline{Y} \leqslant 0.995$, where $\overline{Y}$ is a planar average in x_1-x_2 planes. Only the computational domain in the vicinity of the flame brush is shown.

here corresponds to case F1 first studied in Ref. [22], with the important distinction that the present DNS is performed using temperature-dependent viscosity and turbulence is fully resolved in all regions of the flow.

III. SPECTRAL KINETIC ENERGY DYNAMICS

The effects of premixed flames on interscale energy transfer are analyzed in the present study using the SKE transport equation for compressible reacting flows. The dynamics represented by this equation are predominantly governed by physical processes associated with interactions of three wave vectors, known as triadic interactions (see Refs. [4–9] and references therein), which are a combination of physical-space and spectral-space two-point cross-correlations. Variations of these interactions through the turbulent flame brush are directly indicative of modifications to energy transfer processes by heat release from the flame.

The transport equation for SKE in compressible reacting flows is obtained from the Fourier transform of the compressible Navier-Stokes equation given by

$$\frac{\partial u_i}{\partial t} = \underbrace{-u_j \frac{\partial u_i}{\partial x_j}}_{\mathcal{T}_i} \underbrace{-\frac{1}{\rho}\frac{\partial p}{\partial x_i}}_{\mathcal{P}_i} \underbrace{+\frac{2}{\rho}\frac{\partial}{\partial x_j}\left[\mu\left(S_{ij} - \frac{1}{3}S_{kk}\delta_{ij}\right)\right]}_{\mathcal{V}_i} \underbrace{+\frac{1}{\rho}\frac{\partial}{\partial x_i}\left(\frac{5}{3}\mu S_{kk}\right)}_{\mathcal{D}_i}, \tag{11}$$

where $\mathcal{T}_i$ represents nonlinear advective processes, $\mathcal{P}_i$ represents pressure gradient effects, $\mathcal{V}_i$ represents shear viscous diffusion, and $\mathcal{D}_i$ represents dilatational viscous effects.

In nearly all practical reacting flows, the lack of three homogeneous directions prevents the use of the 3D Fourier transform in obtaining the SKE transport equation. However, since the present analysis is focused on statistically planar premixed flames, for which the flame and turbulent flow are homogeneous and periodic in two dimensions, 2D Fourier transforms can be applied to analyze the full 3D dynamics in each x_1-x_2 plane. A similar approach was employed by Domaradzki *et al.* [8] for the study of turbulent channel flow and by Kolla *et al.* [2] for the study of shear-driven premixed reacting flows. The resulting equation for the velocity spectrum $\widehat{u}_i(\boldsymbol{\kappa},x_3,t)$ is obtained from Eq. (11) as

$$\frac{\partial \widehat{u}_i}{\partial t} = \widehat{\mathcal{T}}_i + \widehat{\mathcal{P}}_i + \widehat{\mathcal{V}}_i + \widehat{\mathcal{D}}_i, \tag{12}$$

where $\widehat{(\cdot)}$ denotes a 2D Fourier transform, $\boldsymbol{\kappa} = [\kappa_1,\kappa_2]$ is the 2D wave vector, and all of the terms in the above equation depend on $\boldsymbol{\kappa}$, x_3, and t.

The SKE at different locations in the flame brush is defined as $\widehat{E}(\boldsymbol{\kappa},x_3,t,\overline{Y}) \equiv \langle \frac{1}{2}\widehat{u}_i^*\widehat{u}_i \mid \overline{Y}\rangle$, where, most generally, $\langle\cdot\rangle$ denotes an ensemble average and $\langle\cdot \mid \overline{Y}\rangle$ denotes conditional averaging on $\overline{Y}(x_3,t)$, the x_1-x_2 planar average of the reactant mass fraction Y. The present definition of SKE corresponds to mass-specific SKE, and thus represents the spectral power of the kinematic velocity field. This approach is appropriate here due to the present focus on interactions between different scales of turbulent motion, as well as to the lack of a mean density gradient in the x_1 and x_2 directions (since the flame is statistically planar). There is also currently no established analytical framework for density-weighted triadic interactions that can be mathematically related to the SGS flux arising from density-weighted filtering operators used in typical combustion LES [2].

A budget equation for SKE can be obtained from

$$\frac{\partial \widehat{E}}{\partial t} \equiv \frac{\partial}{\partial t}\left\langle \frac{1}{2}\widehat{u}_i^*\widehat{u}_i \;\middle|\; \overline{Y}\right\rangle = \left\langle \frac{\partial(\frac{1}{2}\widehat{u}_i^*\widehat{u}_i)}{\partial t} \;\middle|\; \overline{Y}\right\rangle, \tag{13}$$

where the time derivative approximately commutes with the conditional average provided that the rate of change of $\overline{Y}$ is much slower than the rate of change of $\frac{1}{2}\widehat{u}_i^*\widehat{u}_i$, as is the case in the present study (additional detail on the commutativity of the time derivative and the conditional average is provided in the Appendix). In the present analysis, both the flame and turbulence are statistically stationary with respect to an inertial reference frame moving at the average turbulent flame speed. There is a direct correspondence between x_3 and $\overline{Y}$ in this frame, and thus $\overline{Y}$ alone, rather than x_3, can be used to indicate location in the flame brush. As a result, the ensemble conditional average can be replaced by a spatial-temporal conditional average, which then allows Eq. (13) to be rewritten as

$$\frac{\partial \widehat{E}}{\partial t} = \left\langle \frac{1}{2}\left(\widehat{u}_i^*\frac{\partial \widehat{u}_i}{\partial t} + \widehat{u}_i\frac{\partial \widehat{u}_i^*}{\partial t}\right) \;\middle|\; \overline{Y}\right\rangle = 0, \tag{14}$$

where $\partial\widehat{E}/\partial t = 0$ follows from the statistical stationarity of the flow and $\langle\cdot\rangle$ now denotes an average over all x_3 and t. Substituting Eq. (12) into Eq. (14) then gives the transport equation for $\widehat{E}$ in a statistically stationary flow as

$$\frac{\partial \widehat{E}}{\partial t} = \widehat{T} + \widehat{P} + \widehat{V} + \widehat{D} = 0. \tag{15}$$

Here the terms on the right are given generically as $\widehat{G}(\boldsymbol{\kappa},\overline{Y}) = \langle \frac{1}{2}(\widehat{u}_i^*\widehat{\mathcal{G}}_i + \widehat{u}_i\widehat{\mathcal{G}}_i^*) \mid \overline{Y}\rangle$, where $\widehat{G}$ represents $\widehat{T}$, $\widehat{P}$, $\widehat{V}$, or $\widehat{D}$, and $\widehat{\mathcal{G}}_i$ represents $\widehat{\mathcal{T}}_i$, $\widehat{\mathcal{P}}_i$, $\widehat{\mathcal{V}}_i$, or $\widehat{\mathcal{D}}_i$. Terms in Eq. (15) have no dependence on x_3 or t due to the use of a spatial-temporal average.

In the present analysis, 12 different values of $\overline{Y}$ are used in the conditional statistics, corresponding to $\overline{Y} = \{0.00,0.05,0.15,...,0.95,1.00\}$. Furthermore, since the dominant anisotropic direction in the flow is along the x_3 axis, spectral quantities calculated in homogeneous x_1-x_2 planes are isotropic with respect to the wave vector $\boldsymbol{\kappa}$. Therefore, the discrete isotropic SKE, denoted $\widehat{E}_\kappa(\kappa,\overline{Y})$, can be calculated by summing $\widehat{E}(\boldsymbol{\kappa},\overline{Y})$ within wave-number spherical shells of width Δ_κ located at a radius κ, where $\kappa \equiv |\boldsymbol{\kappa}|$ is the wave-vector magnitude. With this, $\widehat{E}_\kappa$ becomes a function of the shell-centered κ values, $\kappa = \{0.25,1,2,...\}\Delta_\kappa$, representing the continuous wave-number shells $[0,\frac{\Delta_\kappa}{2})$, $[\frac{\Delta_\kappa}{2},\frac{3\Delta_\kappa}{2})$, and so on. Similar expressions can be obtained for $\widehat{T}_\kappa$, $\widehat{P}_\kappa$, $\widehat{V}_\kappa$, and $\widehat{D}_\kappa$, each of which depends on κ and $\overline{Y}$.

When one of the shell-integrated terms on the right-hand side of Eq. (15) is positive (i.e., $\widehat{G}_\kappa > 0$) for a particular wave number κ at a particular flame brush location $\overline{Y}$, then the associated physical process contributes to an increase in SKE at that κ and $\overline{Y}$. Conversely, when $\widehat{G}_\kappa < 0$, the associated physical process contributes to a decrease in SKE at that κ and $\overline{Y}$. Note, however, that these terms only indicate whether a particular wave-number shell receives or donates energy as a result of a particular process. They do not specify in which direction (i.e., up-scale, down-scale, or between flame brush locations) the net transfer takes place.

The transport terms in Eq. (15) consist of both in-plane (i.e., within the x_1-x_2 plane at a single $\overline{Y}$) and out-of-plane (i.e., between different $\overline{Y}$ planes) contributions. These contributions to the overall transport can, however, be computed separately. In-plane advective transfer, denoted $\widehat{T}_\kappa^{\parallel}(\kappa,\overline{Y})$, includes only x_1 and x_2 spatial derivatives in Eq. (11) and omits x_3 derivatives. The subfilter-scale flux, which is of primary importance in turbulence modeling for LES, can then be estimated from $\widehat{T}_\kappa^{\parallel}(\kappa,\overline{Y})$ as

$$\Pi(\kappa,\overline{Y}) = \sum_{\kappa'=0}^{\kappa} \widehat{T}_\kappa^{\parallel}(\kappa',\overline{Y}), \tag{16}$$

where $\Pi(\kappa,\overline{Y})$ is the 2D in-plane equivalent of the 3D isotropic spectral flux [9]. The out-of-plane transport must be removed from the computation of Π in order to estimate the flux of energy to subfilter-scales at a given κ, since only the in-plane transport term describes energy transfer purely between wave-number shells at a single $\overline{Y}$. When $\Pi > 0$, the wave-number shell at $(\kappa,\overline{Y})$ is a net recipient of energy from all smaller scales (i.e., higher wave numbers), whereas when $\Pi < 0$, the shell at $(\kappa,\overline{Y})$ is a net donor of energy to all smaller scales.

In order to determine the exact origin and destination of interscale energy transfer, triadic interactions must be

computed. Triadic interactions are the building blocks of multiscale SKE transport and involve interactions between three wave vectors, $\boldsymbol{\kappa}$, $\boldsymbol{\zeta}$, and $\boldsymbol{\xi}$, which form a closed triad $\boldsymbol{\xi} = \boldsymbol{\kappa} - \boldsymbol{\zeta}$. Triadic terms can be found in each of the integrals used to obtain $\widehat{T}$, $\widehat{P}$, $\widehat{V}$, and $\widehat{D}$ in Eq. (15). The energy cascade process is, however, most directly associated with triads comprising the spectral advective transfer term $\widehat{T}$, which is the primary focus of the present study. These particular triads represent self-interactions between three wave vectors of velocity, where a Fourier coefficient of velocity represents the amplitude and phase of a plane wave in the velocity field and the wave vector of the coefficient represents the scale (or wavelength) and direction of the plane wave. As a result, advective triadic interactions are directly connected to the transfer of energy between specific scales of motion due to nonlinear inertial processes. Individual triadic contributions to $\widehat{T}^{\parallel}$ are given by

$$\widehat{T}'^{\parallel}(\boldsymbol{\kappa},\boldsymbol{\zeta},\overline{Y}) = \left\langle -\frac{i}{2}[\widehat{u}_i^*(\boldsymbol{\kappa})\widehat{u}_j(\boldsymbol{\zeta})\xi_j\widehat{u}_i(\boldsymbol{\xi}) + \widehat{u}_i(\boldsymbol{\kappa})\widehat{u}_j^*(\boldsymbol{\zeta})\xi_j\widehat{u}_i^*(\boldsymbol{\xi})]\middle|\overline{Y}\right\rangle, \tag{17}$$

for $i \in \{1,2,3\}$ and $j \in \{1,2\}$. Integration of $\widehat{T}'^{\parallel}(\boldsymbol{\kappa},\boldsymbol{\zeta},\overline{Y})$ over all possible $\boldsymbol{\zeta}$ gives the net spectral transfer $\widehat{T}^{\parallel}(\boldsymbol{\kappa},\overline{Y})$, which is the in-plane component of the advective transfer $\widehat{T}(\boldsymbol{\kappa},\overline{Y})$ appearing in Eq. (15).

Wave vectors can be combined via shell integration in order to derive discrete isotropic transport terms, resulting in the spectral shell relations given by

$$\widehat{T}_{\kappa}^{\parallel}(\kappa,\overline{Y}) = \sum_{\zeta}\widehat{T}'^{\parallel}_{\kappa\zeta}(\kappa,\zeta,\overline{Y})\Delta_{\zeta} = \sum_{\zeta}\sum_{\xi}\widehat{T}'^{\parallel}_{\kappa\zeta\xi}(\kappa,\zeta,\xi,\overline{Y})\Delta_{\zeta}\Delta_{\xi}, \tag{18}$$

where $\zeta \equiv |\boldsymbol{\zeta}|$, $\xi \equiv |\boldsymbol{\xi}|$ becomes an independent variable within the range $|\kappa - \zeta| \leqslant \xi \leqslant |\kappa + \zeta|$, and Δ_{ζ} and Δ_{ξ} represent wave-number shell widths. In Eq. (18), the intermediate quantity $\widehat{T}'^{\parallel}_{\kappa\zeta}$ is given by summing over all ξ as

$$\widehat{T}'^{\parallel}_{\kappa\zeta}(\kappa,\zeta,\overline{Y}) = \sum_{\xi}\widehat{T}'^{\parallel}_{\kappa\zeta\xi}(\kappa,\zeta,\xi,\overline{Y})\Delta_{\xi}. \tag{19}$$

This quantity can be interpreted as a measure of the energy exchange between the wave numbers κ and ζ [6], at a particular $\overline{Y}$ location. Specifically, $\widehat{T}'^{\parallel}_{\kappa\zeta}$ is negative when κ gives energy to a particular ζ, and $\widehat{T}'^{\parallel}_{\kappa\zeta}$ is positive when κ receives energy from a particular ζ.

It should be noted that the summation over ξ in Eq. (19) can be split into various contributions, revealing further insights into the underlying physics. For example, Brasseur and Wei [7] categorize $\widehat{T}'_{\kappa\zeta\xi}(\kappa,\zeta,\xi,\overline{Y})$ into local, nonlocal, and distant triads, where local triads correspond to $\kappa \approx \zeta \approx \xi$, distant triads correspond to $\kappa \ll \zeta \sim \xi$ or $\kappa \sim \xi \ll \zeta$, and all other triads are considered nonlocal. Positive and negative values of $\widehat{T}'_{\kappa\zeta\xi}(\kappa,\zeta,\xi,\overline{Y})$ may also be grouped together in order to separately identify up-scale (i.e., backscatter) and down-scale (i.e., forward-scatter) contributions to the net direction of energy transfer [5]. In the present study, however, the focus is solely on the net direction and magnitude of energy transfer by advective processes, and so we do not perform any local/nonlocal/distant or positive/negative groupings of the triads. Consequently, discussion of advective energy transfer here and in the following refers to the *net* transfer of energy between scales.

It is emphasized that even though triadic interscale interactions are present for each of the energy transfer terms in Eq. (15), the present analysis is focused specifically on triads and energy transfer due to nonlinear advective processes. Nonlinear advection is responsible for moving energy from one velocity scale to another and is thus of considerable importance in the energy cascade process. The analysis of energy transport due to the other terms in Eq. (15) is the subject of future work.

IV. RESULTS

Figure 4 shows SKE for 12 values of $\overline{Y}$ ranging from pure reactants (i.e., $\overline{Y} = 1$), through ten locations inside the flame brush, to pure products (i.e., $\overline{Y} = 0$). Each spectrum is normalized by the forcing-scale SKE in nonreacting HIT of premixed reactants, $\widehat{E}_{\kappa,\mathrm{HIT}}(\kappa = L^{-1})$, with the same turbulence properties as the unburnt reactants (see Table I). This allows a direct comparison to be made of the intensity and scaling of nonreacting and reacting turbulence with identical pre-reaction properties. It should be noted that data corresponding to $\overline{Y} = 0$ and 1 are sampled from just downstream and upstream of the turbulent flame brush, and therefore are not isolated from heat release effects such as pressure pulsations [24] and dilatation [see Fig. (3)].

The spectra in Fig. 4 undergo substantial changes through the flame brush from reactants to products, displaying a suppression of small-scale motions and an enhancement of the mean flow near the products. The suppression of small-scale motions is due to dilatational effects resulting from fluid

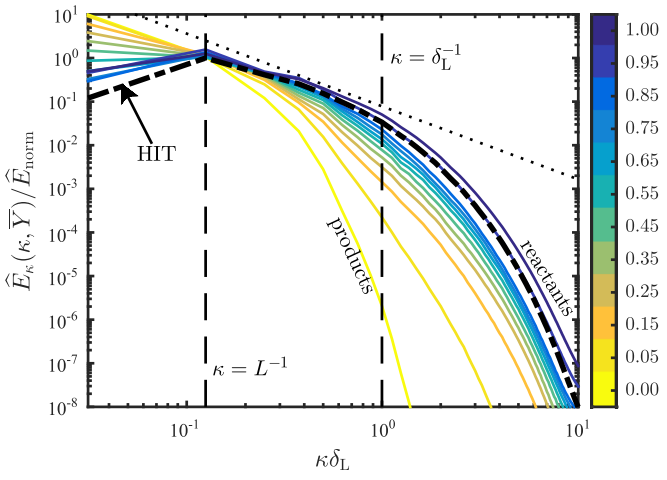

FIG. 4. Isotropic turbulent spectral kinetic energy (SKE), $\widehat{E}_{\kappa}$, normalized by the forcing-scale SKE in nonreacting homogeneous isotropic turbulence (HIT) of premixed reactants, $\widehat{E}_{\mathrm{norm}} \equiv \widehat{E}_{\kappa,\mathrm{HIT}}(\kappa = L^{-1})$. Spectra are colored by $\overline{Y}$ location, with the HIT SKE shown as a heavy black line. Vertical dashed lines correspond to the wave numbers of the domain width L and the laminar thermal flame width δ_{L}. The dotted line shows a $\kappa^{-5/3}$ spectral slope.

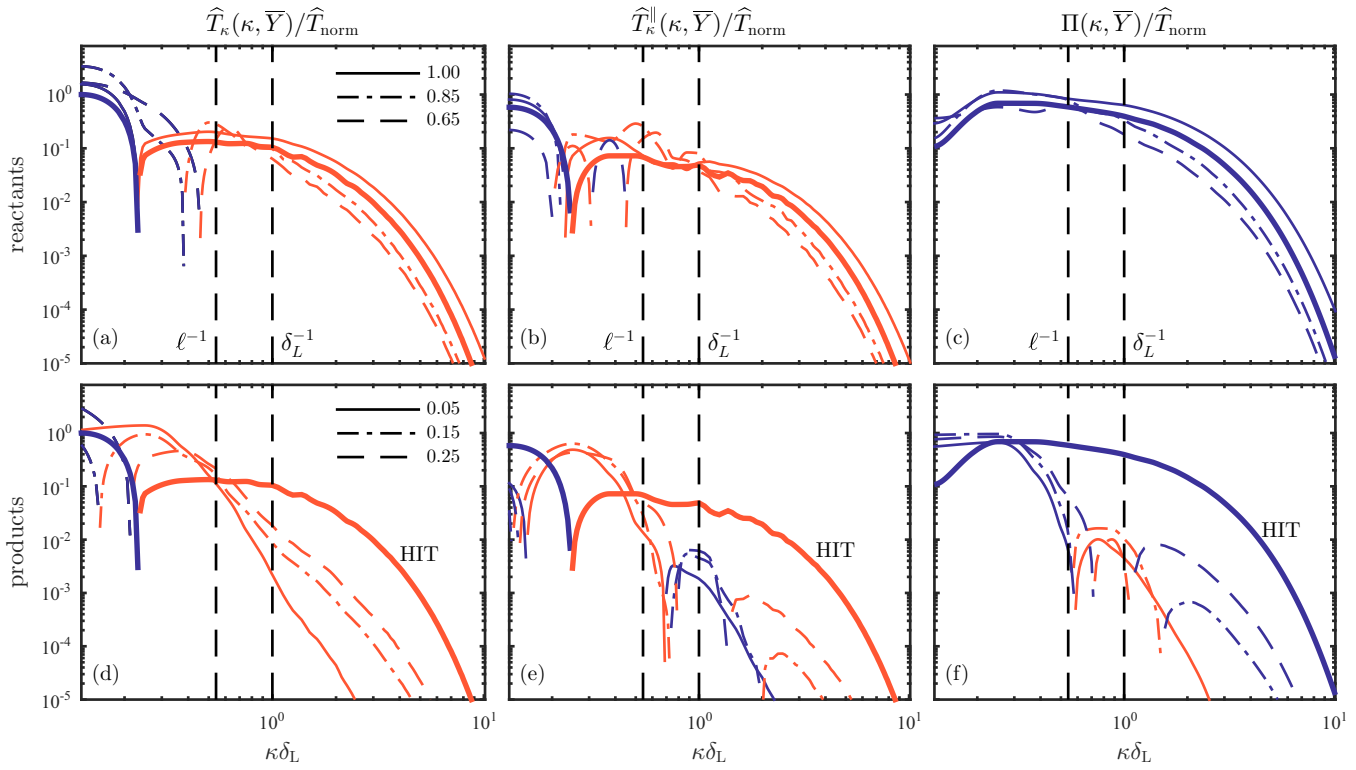

FIG. 5. Total isotropic advective transport, $\widehat{T}_\kappa$, (a) and (d), isotropic in-plane advective transport, $\widehat{T}_\kappa^{\parallel}$, (b) and (e), and isotropic spectral flux, Π, (c) and (f), normalized by the forcing-scale isotropic advective transport in nonreacting HIT of premixed reactants, $\widehat{T}_{\rm norm}=\widehat{T}_{\kappa,{\rm HIT}}(\kappa=L^{-1})$. Panels (a)–(c) correspond to locations near the reactants and panels (d)–(f) correspond to locations near the products. All panels show the absolute values of all quantities. In (a), (b), (d), and (e), orange (light gray) line segments represent a positive contribution to SKE at a particular wave number and blue (dark gray) line segments represent a negative contribution. In (c) and (f), orange (light gray) line segments represent a positive energy flux at a particular wave number and blue (dark gray) line segments represent a negative energy flux. HIT results are shown as heavy solid lines in all panels. Vertical dashed lines show the wave numbers corresponding to the turbulence integral scale, ℓ, and the laminar flame thermal width, $\delta_{\rm L}$.

expansion and the decrease in local Reynolds number resulting from the increase in viscosity. As noted in Sec. I, both of these effects are fundamentally due to heat release by the flame. By the time the flow has crossed the flame, very little evidence remains of the $\kappa^{-5/3}$ inertial range scaling that is present in both the reactants and HIT.

Although changes to the spectra shown in Fig. 4 suggest that interscale energy transfer inside the flame brush may deviate from that found in nonreacting incompressible turbulence, these spectra do not provide any direct information on the specific nature of net energy transfer. Such information, however, is provided in Fig. 5, which shows spectra of the total isotropic advective transport, $\widehat{T}_\kappa$, the in-plane isotropic advection, $\widehat{T}_\kappa^{\parallel}$, and the isotropic spectral flux, Π, normalized by the forcing-scale total isotropic advective transport in nonreacting HIT of premixed reactants, $\widehat{T}_{\kappa,{\rm HIT}}(\kappa=L^{-1})$.

The spectra of $\widehat{T}_\kappa$ in Figs. 5(a) and 5(d) show that, qualitatively, the total isotropic advective transport changes little through the flame brush, with large scales close to the domain width supplying kinetic energy to the full range of smaller scales. Quantitative differences in $\widehat{T}_\kappa$ are attributable, at least in part, to the decrease in Reynolds number from reactants to products. However, when only the in-plane component of $\widehat{T}_\kappa$ is considered [i.e., Figs. 5(b) and 5(e)], there is substantially more variation in the interscale transport dynamics. In particular, $\widehat{T}_\kappa^{\parallel}$ shows little qualitative variation with position in the flame brush near the reactants, but near the products there is a reversal of the net transport at scales near the laminar flame thermal width $\delta_{\rm L}$.

This reversal, which represents net energy backscatter near $\delta_{\rm L}$, is also evident in Fig. 5(f), which shows that Π is positive at scales close to $\delta_{\rm L}$ near the products, indicative of net spectral backscatter of energy from scales smaller than $\delta_{\rm L}$. By contrast, Fig. 5(c) shows that near the reactants, there is no net backscatter of energy at any scale and the results are very similar to those obtained for nonreacting HIT. It is emphasized that the backscatter referred to here is *net* backscatter that consists of both down-scale and up-scale energy transfer due to advective processes. Figure 5(f) indicates that such net spectral backscatter occurs near the products close to the scale of the flame width $\delta_{\rm L}$.

The specific scales of motion contributing to up-scale transfer of energy at a particular wave number can be determined from $\widehat{T}_{\kappa\zeta}^{\prime\parallel}$, which is the in-plane transfer of energy between wave numbers κ and ζ. Figure 6 shows the detailed interactions between all ζ and κ pairs down to scales four times smaller than $\delta_{\rm L}$ for nonreacting HIT and for flame brush locations centered at $\overline{Y}=\{0.15,0.35,1.00\}$, all normalized by the forcing-scale total isotropic advective transport in the nonreacting HIT of premixed reactants, $\widehat{T}_{\kappa,{\rm HIT}}(\kappa=L^{-1})$. Comparison of Figs. 6(a)

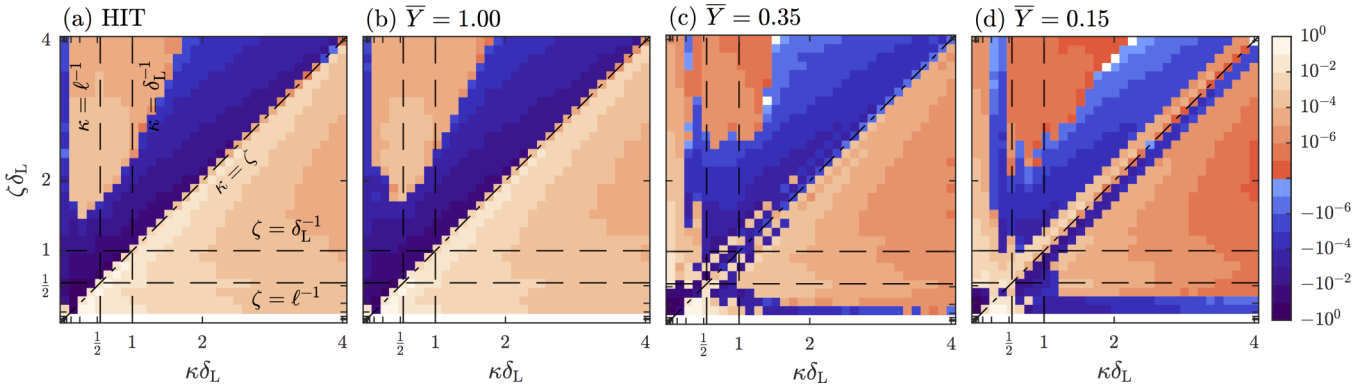

FIG. 6. In-plane, interscale advective transport, $\widehat{T}'^{\parallel}_{\kappa\zeta}$, normalized by the forcing-scale advective transport for nonreacting HIT in premixed reactants, $\widehat{T}_{\text{norm}} = \widehat{T}_{\kappa,\text{HIT}}(\kappa = L^{-1})$. Orange (light gray) at a particular (κ,ζ) coordinate indicates that wave number κ receives energy from wave number ζ, while blue (dark gray) indicates that κ donates energy to ζ. Dashed lines correspond to ℓ and δ_L, and the dash-dot line shows $\kappa = \zeta$. Panels show results for (a) HIT, and flame brush locations corresponding to (b) $\overline{Y} = 1.00$, (c) $\overline{Y} = 0.35$, (d) $\overline{Y} = 0.15$.

and 6(b) shows that at flame brush locations near the reactants, interscale advective energy transfer is similar to that found in HIT. In both cases, generally positive values of $\widehat{T}'^{\parallel}_{\kappa\zeta}$ occur for $\zeta < \kappa$ and negative values occur for $\zeta > \kappa$, corresponding to a down-scale transfer of energy from large to small scales (i.e., low to high wave numbers). Near the products, however, Figs. 6(c) and 6(d) show that close to the main diagonal where $\zeta = \kappa$, the direction of energy transfer is reversed, with positive values of $\widehat{T}'^{\parallel}_{\kappa\zeta}$ for $\zeta > \kappa$ and negative values for $\zeta < \kappa$. This reversal is, once again, indicative of net energy backscatter from small to large scales (i.e., high to low wave numbers), and is most pronounced near the scale δ_L.

Net advective energy backscatter near scale δ_L can be seen more clearly by taking one-dimensional profiles of $\widehat{T}'^{\parallel}_{\kappa\zeta}$ from Figs. 6(b) and 6(d) at $\kappa\delta_L = 0.625$, 1, and 1.375, where $\kappa\delta_L = 1$ corresponds to the scale of the laminar flame thermal width. The resulting curves, shown in Fig. 7, give the contributions of different wave numbers ζ to the energy associated with wave number κ. In particular, Fig. 7(a) shows that near the reactants, there is a down-scale transfer of energy from large to small scales (i.e., low to high wave numbers) for each κ, with wave number κ receiving energy from wave numbers $\zeta < \kappa$ and donating energy to wave numbers $\zeta > \kappa$. The collection of curves shown in Fig. 7(a) thus represents a net forward cascade of energy from large to small scales.

At locations in the flame brush near the products, by contrast, the direction of energy transfer is reversed, with wave number κ donating energy to wave numbers $\zeta < \kappa$ and receiving energy from wave numbers $\zeta > \kappa$. The strength of the resulting net energy backscatter is, however, substantially weaker than the down-scale transfer near the reactants shown in Fig. 7(a). The substantial reduction in magnitude of the triadic transfer terms is also evident in the overall lower magnitudes of $\widehat{T}'^{\parallel}_{\kappa\zeta}$ shown in Fig. 6(d) near the products. Consequently, net transfer rates near the products are much smaller in magnitude compared to rates near the reactants, regardless of the direction in which the transfer occurs. For low ζ, the curve for $\kappa\delta_L = 0.625$ in Fig. 7(b) exhibits down-scale energy transfer, and at even smaller values of κ, shown in Fig. 6(d), essentially all up-scale transfer of energy is lost, even for locations near the products. As a result, Fig. 7(b) provides clear evidence of net advective energy backscatter for scales near the flame width δ_L in premixed reacting flows, but also shows that the resulting inverse cascade of energy does not extend to the scale of the domain width.

This last point is shown more clearly in Figs. 5(f) and 6(d), both of which indicate that up-scale energy transfer by advective processes terminates at scales near the turbulence integral scale ℓ, and for larger scales there is a net down-scale transfer of energy (although this down-scale energy transfer is much weaker than in the reactants or in HIT). These results thus suggest that while up-scale energy transfer and net backscatter do occur in premixed reacting flows, advective processes may not be effective at creating an inverse cascade that extends past the turbulence integral scale; further analysis of this result requires additional, computationally expensive, simulations where ℓ is made much larger than δ_L.

V. SUMMARY AND CONCLUSIONS

In the present analysis, the effects of premixed flames on spectral properties of turbulence have been quantified using 2D Fourier transforms and statistics conditioned on location in the flame brush. The analysis is based on data from a well-resolved DNS of a 3D statistically planar premixed flame in which the laminar flame width is resolved with 64 computational grid cells and the turbulent Kolmogorov scale is resolved everywhere in the domain with at least two grid cells.

Changes to the turbulent energy transfer are apparent in the kinetic energy spectra (Fig. 4). In particular, these spectra vary significantly between locations in the flame brush near the reactants and locations near the products, with a substantial suppression of small-scale motions and an increase in the mean flow kinetic energy occurring in the products. Calculation of triadic interactions between different scales of fluid motion (Figs. 6 and 7) demonstrates that within the flame brush near the products, there is a reversal of the direction of net advective energy transfer at the scale of the laminar flame thermal width. This results in net advective backscatter of energy from small to large scales, corresponding to positive values of the isotropic spectral flux Π (Fig. 5). These results qualitatively match the results of a physical-space analysis of density-weighted SGS fluxes computed in Ref. [3] using the same DNS data.

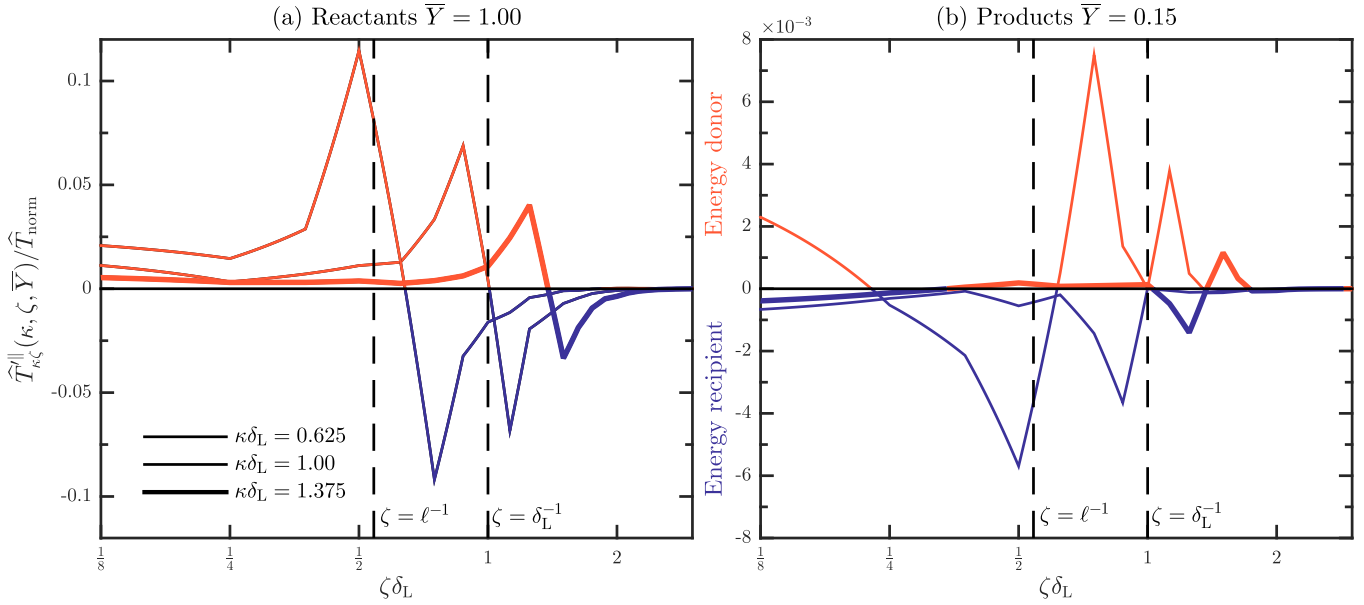

FIG. 7. In-plane advective transport of SKE, $\widehat{T}^{\prime\parallel}_{\kappa\zeta}$, between wave numbers $\kappa\delta_{\mathrm{L}} = [0.625, 1, 1.375]$ and ζ for flame brush locations near (a) the reactants and (b) the products. Positive (negative) values indicate that the scale ζ is a donor (recipient) of SKE to (from) the scale κ.

Analysis of the net spectral flux and triadic interactions near the products [Figs. 5(f) and 6(d)] indicates that net backscatter by advective processes extends up to the turbulence integral scale. Energy injection occurs at scales larger than the integral scale, and such large-scale energy can only be transported to smaller scales (i.e., down-scale). Therefore, at some intermediate scale, backscatter of energy from the flame scale is balanced by forward-scatter of energy from large scales. Further investigation into the possibility of an extended inverse energy cascade over a greater range of scales thus requires additional simulations in a larger domain with greater separation between the energy injection and flame scales. Even so, the present results have immediate relevance for LES modeling, since the presence of a strong forward cascade cannot be assumed at filter scales near the laminar flame thermal width in large spatial regions both within and downstream of the flame brush. Whether or not an LES practitioner should expect current models to deviate significantly from these findings depends on the details of the turbulent combustion process being modeled, as well as the grid scale of the LES performed.

It should be noted that the present spectral analysis is performed in 2D even though both the turbulence and the flame are inherently 3D. While this restricts the analysis of spectral energy transfer and backscatter to statistically homogeneous and isotropic planes perpendicular to the direction of flame propagation, the present results show that within these planes there is a clear transition from uniformly down-scale to locally up-scale advective transfer of energy when moving through the flame brush from reactants to products. In order to perform a fully 3D analysis of spectral backscatter through the flame brush that can be quantitatively compared to Ref. [3], a spatially local scale decomposition must be performed, for example using wavelets. Such an analysis is the subject of future work.

In addition to extending the analysis to 3D, the present study of scale interactions may also be extended in several other directions. In particular, scalar (e.g., reactant mass fraction) spectra are an important aspect of theories for turbulent flame speed (see, for example, Refs. [25–31]), and the present analysis approach may yield insights into how such spectra change through premixed flames. In the present study we have also only examined $\mathrm{Le} = 1$ flames, but prior studies (e.g., Refs. [32,33]) have indicated that the strength of dilatational effects may increase as Le decreases. It would thus be interesting in the future to determine how kinetic energy transfer processes are affected by varying Le. Similarly, as ever greater computational resources become available, the results presented herein using single-step premixed chemistry can be re-examined using a multistep chemical mechanism.

Finally, in the present analysis only energy transfer associated with nonlinear advective processes has been examined. Although these processes are most directly connected with turbulent interscale energy transfer, which is the focus of this work, pressure-gradient, variable-density, and variable-viscosity effects also give rise to interscale dynamics in premixed reacting flows. Such effects are represented in Eq. (15) by the terms $\widehat{P}$, $\widehat{V}$, and $\widehat{D}$. These terms may transfer energy between SKE and internal energy, particularly at large scales, and are also an important subject for future work.

ACKNOWLEDGMENTS

Helpful discussions with Dr. Chiping Li, as well as the support of the Stanford Center for Turbulence Research Summer Program, are gratefully acknowledged. C.A.Z.T. and P.E.H. were supported in part by AFOSR Award No. FA9550-14-1-0273 and by the Department of Defense (DoD) High Performance Computing Modernization Program (HPCMP). A.Y.P. was supported in part by AFOSR Award No. F4FGA06055G001 and NASA Award No. NNH12AT33I.

J.U. and M.I. were supported in part by AFOSR Award No. FA9550-14-1-0219. Computing resources were provided by DoD HPCMP under a Frontier project award, and by the Naval Research Laboratory.

APPENDIX: APPROXIMATE COMMUTATION OF DIFFERENTIATION AND CONDITIONAL AVERAGING

The relation in Eq. (13) is obtained by requiring that the time derivative at least approximately commutes with the conditional ensemble average. In the following, we outline the conditions for which this approximate commutation is valid. In particular, it can be shown that the time derivative approximately commutes with the conditional average provided that the rate of change of $\overline{Y}$ is much smaller than the rate of change of $\frac{1}{2}\widehat{u}_i^*\widehat{u}_i$, and that the commutation error decreases with increasing scale separation between the time derivatives of these two quantities.

Introducing the arbitrary random variables X and Y, both of which depend on time t, we seek to show that

$$\frac{d}{dt}\langle X \mid Y\rangle = \left\langle \frac{dX}{dt} \,\middle|\, Y \right\rangle, \tag{A1}$$

where the operator $\langle\cdot\rangle$ is taken here to represent an ensemble average. Beginning with the left-hand side of Eq. (A1), the time derivative of a conditional average at time t can be written using the fundamental theorem of calculus as

$$\frac{d}{dt}\langle X \mid Y\rangle \equiv \lim_{h\to 0} \frac{\langle X(t+h)|Y(t+h)\rangle - \langle X(t-h)|Y(t-h)\rangle}{2h}. \tag{A2}$$

By contrast, application of the fundamental theorem of calculus to the right-hand side of Eq. (A1) gives

$$\left\langle \frac{dX}{dt} \,\middle|\, Y \right\rangle \equiv \lim_{h\to 0} \left\langle \frac{X(t+h)-X(t-h)}{2h} \,\middle|\, Y(t) \right\rangle. \tag{A3}$$

Due to the linearity of the conditional average, this expression can be further rewritten as

$$\left\langle \frac{dX}{dt} \middle| Y \right\rangle \equiv \lim_{h\to 0} \frac{\langle X(t+h)|Y(t)\rangle - \langle X(t-h)|Y(t)\rangle}{2h}. \tag{A4}$$

Comparison of Eqs. (A2) and (A4) shows that the primary differences between these two relations are the times at which the conditioning on Y is computed. Using Taylor expansions, however, the conditioning variables $Y(t+h)$ and $Y(t-h)$ can be approximated as

$$Y(t \pm h) \approx Y(t) \pm \frac{dY}{dt}h. \tag{A5}$$

Substituting this expansion into Eq. (A2) then gives

$$\frac{d}{dt}\langle X \mid Y\rangle \approx \lim_{h\to 0} \frac{1}{2h}\left[\left\langle X(t+h)\middle| Y(t) + \frac{dY}{dt}h\right\rangle - \left\langle X(t-h)\middle| Y(t) - \frac{dY}{dt}h\right\rangle\right]. \tag{A6}$$

It is readily apparent from comparison of Eqs. (A4) and (A6) that in the limit of vanishing dY/dt, the time derivative of $X(t)$ commutes exactly with the conditional ensemble average. It is also the case that Eqs. (A4) and (A6) are approximately equal provided that time variations in Y are small relative to those in X, such that

$$\frac{X(t+h)-X(t-h)}{X(t)} \gg \frac{Y(t+h)-Y(t-h)}{Y(t)}, \tag{A7}$$

and therefore $Y(t+h) \approx Y(t) \approx Y(t-h)$.

In the specific case of the premixed reacting flow studied here, the conditioning variable $\overline{Y}(x_3,t)$ is a spatial average in a periodic plane, and therefore can be expected to vary only with the very largest time scales of the flow such as the eddy turnover time, the acoustic domain-crossing time, and the flame self-crossing time. Conversely, the conditioned variable, $\frac{1}{2}\widehat{u}_i^*\widehat{u}_i$, varies with the smallest time scales of the flow, such as the Kolmogorov time micro-scale, the acoustic cell-crossing time, and the characteristic small-scale chemical reaction time. As a result, there should be little error in the commutation of the time derivative and ensemble average in Eq. (13).

[1] R. Knaus and C. Pantano, On the effect of heat release in turbulence spectra of nonpremixed reacting shear layers, J. Fluid Mech. **626**, 67 (2009).

[2] H. Kolla, E. R. Hawkes, A. R. Kerstein, N. Swaminathan, and J. H. Chen, On velocity and reactive scalar spectra in turbulent premixed flames, J. Fluid Mech. **754**, 456 (2014).

[3] J. O'Brien, C. A. Z. Towery, P. E. Hamlington, M. Ihme, A. Y. Poludnenko, and J. Urzay, The cross-scale physical-space transfer of kinetic energy in turbulent premixed flames, *36th International Symposium on Combustion, Seoul, Korea* (https://www.combustioninstitute.org/pages/page348.php, 2016).

[4] J. A. Domaradzki and R. S. Rogallo, Local energy transfer and nonlocal interactions in homogeneous, isotropic turbulence, Phys. Fluids A **2**, 413 (1990).

[5] F. Waleffe, The nature of triad interactions in homogeneous turbulence, Phys. Fluids A **4**, 350 (1992).

[6] Y. Zhou, Degrees of locality of energy transfer in the inertial range, Phys. Fluids A **5**, 1092 (1993).

[7] J. G. Brasseur and C.-H. Wie, Interscale dynamics and local isotropy in high Reynolds number turbulence within triadic interactions, Phys. Fluids **6**, 842 (1994).

[8] J. A. Domaradzki, W. Liu, C. Härtel, and L. Kleiser, Energy transfer in numerically simulated wall-bounded turbulent flows, Phys. Fluids **6**, 1583 (1994).

[9] J. A. Domaradzki and D. Carati, An analysis of the energy transfer and the locality of nonlinear interactions in turbulence, Phys. Fluids **19**, 085112 (2007).

[10] A. N. Kolmogorov, The local structure of turbulence in incompressible viscous fluid for very large Reynolds numbers, Dokl. Akad. Nauk SSSR **30**, 299 (1941).

[11] J. Furukawa, E. Harada, and T. Hirano, Local reaction zone thickness of a high intensity turbulent premixed flame, Symp. (Int.) Comb. **23**, 789 (1990).
[12] J. Furukawa, Y. Noguchi, T. Hirano, and F. A. Williams, Anisotropic enhancement of turbulence in large-scale, low-intensity turbulent premixed propane-air flames, J. Fluid Mech. **462**, 209 (2002).
[13] J. O'Brien, J. Urzay, M. Ihme, P. Moin, and A. Saghafian, Subgrid-scale backscatter in reacting and inert supersonic hydrogen-air turbulent mixing layers, J. Fluid Mech. **743**, 554 (2014).
[14] M. Tanahashi, M. Fujimura, and T. Miyauchi, Coherent fine-scale eddies in turbulent premixed flames, Proc. Comb. Inst. **28**, 529 (2000).
[15] J. B. Bell, R. K. Cheng, M. S. Day, and I. G. Shepard, Numerical simulation of Lewis number effects on lean premixed turbulent flames, Proc. Comb. Inst. **31**, 1309 (2007).
[16] J. M. Stone, T. A. Gardiner, P. Teuben, J. F. Hawley, and J. B. Simon, Athena: A new code for astrophysical MHD, Astrophys. J. Suppl. Series **178**, 137 (2008).
[17] A. Y. Poludnenko and E. S. Oran, The interaction of high-speed turbulence with flames: Global properties and internal flame structure, Combust. Flame **157**, 995 (2010).
[18] A. Y. Poludnenko and E. S. Oran, The interaction of high-speed turbulence with flames: Turbulent flame speed, Combust. Flame **158**, 301 (2011).
[19] V. N. Gamezo, T. Ogawa, and E. S. Oran, Flame acceleration and DDT in channels with obstacles: Effect of obstacle spacing, Combust. Flame **155**, 302 (2008).
[20] N. Peters, *Turbulent Combustion* (Cambridge University Press, Cambridge, UK, 2000).
[21] P. Yeung and S. B. Pope, Lagrangian statistics from direct numerical simulations of isotropic turbulence, J. Fluid Mech. **207**, 531 (1989).
[22] P. E. Hamlington, A. Y. Poludnenko, and E. S. Oran, Interactions between turbulence and flames in premixed reacting flows, Phys. Fluids **23**, 125111 (2011).
[23] P. E. Hamlington, A. Y. Poludnenko, and E. S. Oran, Intermittency in premixed turbulent reacting flows, Phys. Fluids **24**, 075111 (2012).
[24] A. Y. Poludnenko, Pulsating instability and self-acceleration of fast turbulent flames, Phys. Fluids **27**, 014106 (2015).
[25] N. Peters, The turbulent burning velocity for large-scale and small-scale turbulence, J. Fluid Mech. **384**, 107 (1999).
[26] V. Yakhot, Propagation velocity of premixed turbulent flames, Combust. Sci. Technol. **60**, 191 (1988).
[27] A. Pocheau, Scale invariance in turbulent front propagation, Phys. Rev. E **49**, 1109 (1994).
[28] V. Bychkov, Importance of the Darrieus-Landau instability for strongly corrugated turbulent flames, Phys. Rev. E **68**, 066304 (2003).
[29] V. Bychkov, A. Petchenko, and V. Akkerman, On the theory of turbulent flame velocity, Combust. Sci. Technol. **179**, 137 (2007).
[30] S. Chaudhuri, V. Akkerman, and C. K. Law, Spectral formulation of turbulent flame speed with consideration of hydrodynamic instability, Phys. Rev. E **84**, 026322 (2011).
[31] S. Chaudhuri, F. Wu, D. Zhu, and C. K. Law, Flame Speed and Self-Similar Propagation of Expanding Turbulent Premixed Flames, Phys. Rev. Lett. **108**, 044503 (2012).
[32] N. Chakraborty, M. Klein, and N. Swaminathan, Effects of Lewis number on the reactive scalar gradient alignment with local strain rate in turbulent premixed flames, Proc. Combust. Inst. **32**, 1409 (2009).
[33] N. Chakraborty and R. S. Cant, Effects of Lewis number on scalar transport in turbulent premixed flames, Phys. Fluids **21**, 035110 (2009).